2009 American Control Conference
Hyatt Regency Riverfront, St. Louis, MO, USA
June 10-12, 2009

Through the Membrane & Along the Channel Flooding in PEMFCs

Jason B. Siegel and Anna G. Stefanopoulou

Abstract— **Neutron imaging of a polymer electrolyte membrane fuel cell (PEMFC) revealed distinct patterns of water fronts moving through the gas diffusion layers (GDL) and channels [1]. The PEMFC was operating with dead-ended, straight and almost vertically-oriented anode channels; hence the gravity driven accumulation of liquid water at the end of the channel caused flooding in an upward direction. In order to predict the spatiotemporal evolution of water patterns inside severely-flooded fuel cells, various distributed parameter models of the water transport through the membrane and GDLs to the cathode and anode channels have been developed by the authors and others.**

In this paper, a zero-dimensional moving front model is presented which captures the location of the water phase transition inside the GDL, instead of using the standard partial differential equation (PDE) approach for modeling liquid water in porous media which is numerically difficult to solve. This model uses three nonlinear states (the anode and cathode GDL front location and the membrane water content) and three inputs (the anode and cathode vapor concentration and the current density) to predict the slowly evolving front locations in both anode and cathode side GDLs during flooding and drying as well as the dynamic changes in membrane water content. The unit cell model is finally formulated with three hybrid modes and their transition laws. The hybrid-state model will be parameterized in the future using experimentally observed front evolutions. This parameterized unit cell model will be used to model the water accumulation along the channel in order to predict and avoid severe flooding conditions.

Water management is a critical issue for PEMFC operation to ensure long stack life and efficient operation. There needs to be sufficient water content in the membrane, (high λ_{mb}), so that proton conduction through the membrane is easy (a dry membrane has higher resistance which leads to voltage loss), but flooding in the channels or catalyst layers is undesirable, and can cause permenant degradation or damage.

Water produced at the cathode catalyst layer will diffuse back to the anode side due to the gradient in water concentration across the membrane. Unfortunately there is also a concentration gradient for nitrogen, when air is used as fuel on the cathode, which leads to nitrogen diffusion across the membrane and accumulation in the anode channel [2], [3]. During low flows gravity, buoyancy and channel orientation help establish statistically repeatable and large spatiotemporal variations, which allows for model simplification. In the anode channel, water liquid, water vapor and nitrogen will settle to the bottom of the channel and in the extreme case of dead-ended anode operation, these heavier molecules will displace hydrogen from that portion of the cell, leading to voltage loss and carbon corrosion of the catalyst support in the cathode [1], [4], [5], [6]. Therefore scheduling an occasional purge of the anode volume is necessary to remove the accumulated water and inert gas [7], [8]. The control input u, shown in Fig. 1, can be used to adjust the purge period and duration. Too frequent purging wastes hydrogen and may over dry the membrane leading to decreased cell performance and other degradation issues. Hence a model-based purge-schedule is highly desirable.

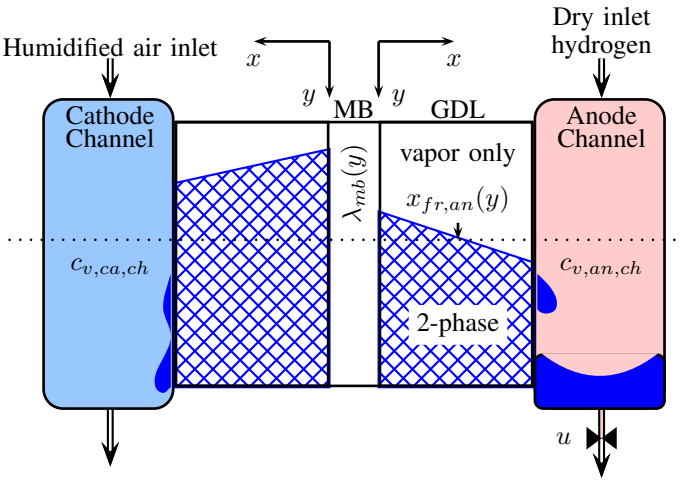

Fig. 1. A schematic of water fronts propagating inside a polymer electrolyte membrane fuel cell motivating the proposed modeling paradigm.

In our previous work we showed that 6 coupled 2nd order partial differential equations (PDEs), three for each side of the membrane, described the 1-D time varying liquid water, water vapor, and reactant gas (hydrogen or oxygen) distribution through the gas diffusion layer GDL [8], [9] and [10]. The previous model, utilized an averaged lumped parameter approach for the channel concentrations which served as boundary conditions for the PDEs. The PDE model with lumped parameter channels demonstrated good results for the majority of operating conditions [8], but the unit cell model with a PDE description requires a very fine discretization grid for liquid water, in order to capture the steep front at the two phase transition. Adaptive grids and other methodologies have been used to handle this type of problem, but they are not well suited for a reduced complexity, control oriented model.

In this paper we leverage the nature of the sharp transition in the GDL liquid water volume. We define the two-phase front location in the GDL, along the x direction, in terms of an ordinary differential equation (ODE), greatly reducing the computational complexity of the 1-D 2-phase water model. The proposed model uses three nonlinear states (the anode

Funding is provided by the National Science Foundation

J. Siegel and A. Stefanopoulou are with the Fuel Cell Control Laboratory, University Michigan, Ann Arbor, MI 48109, USA siegeljb@umich.edu

TABLE I

NOMENCLATURE

Catalyst layer	CTL
Membrane	MB
Gas Diffusion Layer	GDL
Maximum liquid water flux (mol cm^{-2} s^{-1})	$N_{L,max}$
Anode water vapor concentration	$c_{v,an}$
Slope of $c_{v,an}$ in single-phase region	m_v
Y-intercept of $c_{v,an}$ in single-phase region	b_v
Water content of liquid equilibrated membrane	$\lambda_{max} = 22$ [13]
GDL thickness (μm)	$\delta_{GDL} = 420$
Membrane thickness (μm)	$\delta_{mb} = 25$
Mass transfer coefficient	k_{mt}
Channel height (mm)	$H_{ch} = 1$
Vapor flux in the anode GDL	$N_{v,an}$
Liquid saturation in the two phase region	s_*
Catalyst layer liquid water saturation	$s_{ctl,j}$
Temperature (K)	T
Water activity	$a = c_v/c_{v,sat}$
GDL porosity	ϵ=0.8
Vapor diffusivity (cm^2 s^{-1})	$D_V = 0.345$
Porosity corrected vapor diffusivity (cm^2 s^{-1})	$D_{v,e}$ [14]
Sherwood number	$Sh = 2.693$ [15]
Faraday's constant	F
Current density (A cm $^{-2}$)	i_{fc}

and cathode GDL water front location and the membrane water content) and three inputs (the anode and cathode vapor concentration and the current density) to predict the dynamically evolving front locations in both anode and cathode side GDLs during flooding and drying as well as the slower dynamic changes in membrane water content. We present the detailed equations only for the anode and the membrane, and just highlight the modifications necessary for the cathode calculations. The unit cell model is finally formulated with three hybrid modes and their transition laws. Apart from the new modeling paradigm based on moving water fronts, we also show that the water transport through the membrane can be improved by including an additional mechanism for liquid water transport through the membrane similar to [11], [12].

I. PROPOSED MODELING PARADIGM

The liquid water in the GDL is described in terms of liquid saturation $s = v_l/v_p$, which is the ratio of liquid volume to open pore volume. The steep drop in s at the transition between the two-phase and single phase water areas in the GDL is the result of the sigmoidal function of the capillary pressure [14] and requires very fine discretization of the PDEs [8], [10], in order to accurately represent the front propagation. Therefore, we choose to model the liquid water accumulation in the fuel cell using an ODE moving front approach, similar to [16]. We assume that the liquid water propagates at a constant, tunable, volume fraction, s_*, which is slightly larger than the immobile limit.

The caricature shown in Fig. 2, with a square-shape two-phase front highlights the steep transition and the front propagation dx_{fr}/dt. Using the numerical solution of the physically-derived PDEs in [8], [10] and the experimental observations in [1] we infer that locally, liquid water first begins to accumulate in the GDL as shown in frame (a).

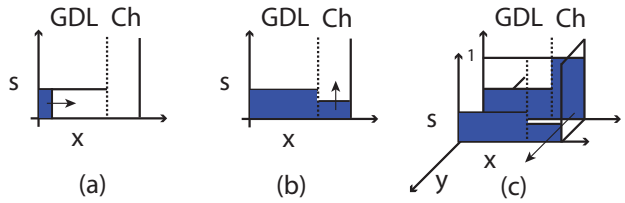

Fig. 2. Evolution of liquid water fronts in the GDL and channel. In frame (a) liquid water fills the GDL up to $s = s_*$, then the two phase front propagates toward the channel. Next in (b) the liquid begins to accumulate in the channel. Finally in (c) once the channel section fills completely water begins to spread back up along the channel.

In the next frame, (b), the liquid water front has reached the GDL-channel boundary. Since there is little resistance to water entering the channel, it begins to spill out of the GDL and into the channel where it accumulates. Finally in frame (c), liquid water fills the anode channel section completely and begins spreading along the y-direction, up the channel and against gravity. Convection and buoyancy dominate transport in the channels due to the long aspect ratio, $L_{ch} >> H_{ch} >> \delta_{GDL}$, therefore we only need to be concerned with modeling the front locations and parameter variation in the y direction for the channel domain after stacking the unit cell equations devoped here.

In the following section we introduce the ordinary differential equations that describe the water dynamics in the membrane and the water front in the GDLs. The model is implemented as a three-mode hybrid-state model and will be stacked (literally and figuratively) in the future to model the water front propagation in the channels.

II. SYSTEM EQUATIONS 0-D UNIT FUEL CELL MODEL

The water dynamics in the GDL-MB-GDL unit model are governed by the membrane water content and the location of a liquid water front in the GDLs as follows. A single state can be used to model water uptake into the membrane. Diffusion within the membrane is fast with respect to water uptake, therefore we can solve the diffusion and osmotic drag in each half of the membrane, using (5) and (13), which yields a piecewise linear water content profile as indicated in Fig 3. The average membrane water content, λ_{mb}, is calculated from the water flux into the membrane from the cathode side, $N_{v,ca,mb}$, and out of the membrane from the anode side, $N_{v,an,mb}$,

$$\frac{d\lambda_{mb}}{dt} = K_{mb}(N_{v,ca,mb} - N_{v,an,mb}) \,, \tag{1}$$

where $K_{mb} = EW/(\rho_{mb}\,\delta_{mb})$ is the membrane water uptake rate.

The location of the two phase (liquid-vapor) water front in the anode GDL, $x_{fr,an}$, is governed by the rate of water accumulation in the GDL that is condensing into the liquid phase, $N_{l,an}$. Hence the front propagation is given by,

$$\frac{\mathrm{d}x_{fr,an}}{\mathrm{d}t} = K_L \begin{cases} N_{l,an} & x_{fr,an} < \delta_{GDL} \\ \min(0, N_{l,an}) & x_{fr,an} = \delta_{GDL} \end{cases}, \tag{2}$$

where $K_L = M_v/(\rho_l\ s_*\ \epsilon\ \delta_{GDL})$ is a constant which accounts for the geometry and density of liquid water in the two phase region assuming the front propagates with constant liquid saturation ($s = s_*$), as shown in Fig. 3. The right hand side (RHS) of (2) depends on $N_{l,an}$, which is equal to the difference between the flux of water entering the GDL from the membrane, $N_{v,an,mb}$, and the flux of vapor leaving from the GDL and entering the channel $N_{v,an}$,

$$N_{l,an} = N_{v,an,mb} - N_{v,an}\ . \tag{3}$$

These fluxes are diffusive fluxes and hence depend on the vapor profile in the GDL, $c_{v,an}(x)$ which in turn depends on the liquid phase front location $x_{fr,an}$.

This spatially and temporally dependent coupling between the liquid and vapor phase through the condensation and evaporation is simplified in this paper by employing two assumptions. First, the liquid water dynamics are much slower than the gas dynamics, due to the difference in density, 1000 times greater. Therefore, for the purpose of tracking the liquid front propagation in the fuel cell, we can take the gas states to be in steady state [10], [16]. Second, we assume that all the condensation and evaporation occurs at the membrane-GDL (MB-GDL) $x = 0$ and liquid phase front location $x_{fr,an}$. With these assumptions, the steady-state solution of the vapor diffusion equation is a piece-wise linear profile for the water vapor concentration, which follows the liquid water front location as seen in Fig. 3,

$$c_{v,an}(x) = \begin{cases} \min(b_v, c_{v,sat}(T)) & x \le x_{fr,an} \\ m_v\ x + b_v & x > x_{fr,an}\ . \end{cases} \tag{4}$$

The vapor profile, $c_{v,an}(x)$, behind the front in the two phase region $x \le x_{fr,an}$ is equal to the concentration at saturation $c_{v,sat}(T)$. In the vapor phase region, between the front location and the channel $x > x_{fr,an}$, the linear profile is the result of Fickian diffusion, and is discussed more in Sec. II-B.

The propagation of the front location in the cathode GDL, $\dot{x}_{fr,ca}$, is defined similarly, where $N_{l,ca}$ is given by (12). For brevity only the equations detailing the anode side will be presented, the cathode side equations are similar except where noted. The system can be described using an isothermal model or a slowly evolving temperature profile where the measured end plate temperature is imposed as the boundary condition at the GDL-channel (GDL-ch) interface and a few degrees higher (load dependent) temperature at the membrane-GDL (MB-GDL) interface because heat is generated from the reaction. Here we assume a spatially invariant temperature distribution and present the equations with explicit temperature dependencies only when variables are first introduced.

A. Membrane Water Transport

The water flux out of the membrane and into the anode GDL is governed by diffusion and osmotic drag,

$$N_{v,an,mb} = 2\,\frac{\alpha_w\ D_w(\lambda_{mb}, T)\ \cdot\ (\lambda_{mb} - \lambda_{an})}{\delta_{mb}} - \frac{n_d\ i_{fc}}{F}\ . \tag{5}$$

The first term in (5) describes diffusion in the membrane, which is driven by the anode side gradient of the membrane water concentration as it is shown in Fig. 3. The anode water gradient is defined by the state, λ_{mb}, and the water content at the membrane interface with the anode GDL λ_{an}. In reality, at the MB-GDL interface there is a catalyst layer, but since the catalyst layer is very thin its effect can be lumped into λ_{an}. Therefore we express λ_{an} as a function of catalyst flooding level, $s_{ctl,an}$ and the vapor concentration in the GDL $c_{v,an}(0)$,

$$\lambda_{an} = (1 - s_{ctl,an})\ \lambda_{T,a} + s_{ctl,an}\ \lambda_{max}, \tag{6}$$

where $\lambda_{T,a}$ is the membrane water uptake isotherm [8], [17],

$$\lambda_{T,a} = c_0(T) + c_1(T)\ a + c_2(T)\ a^2 + c_3(T)\ a^3, \tag{7}$$

which is a function of the water activity, a, at the GDL-MB interface. The water activity in the GDL-MB interface is equal to the ratio of vapor concentration to the saturation value, $a = c_{v,an}(0)/c_{v,sat}$.

The dependece of membrane water content on catalyst liquid saturation is introduced to capture the observed anode flooding behavior. We propose that $s_{ctl,an}$ is a function of the liquid flux $N_{l,an}$ as follows,

$$s_{ctl,an} = \frac{\max(N_{l,an}, 0)}{N_{L,max}}, \tag{8}$$

where $N_{L,max}$ is the maximum liquid water flux the catalyst layer can handle before becoming completely saturated. $N_{L,max}$ should be inversely proportional to liquid water viscosity, therefore we choose the following functional form with an exponential temperature dependence,

$$N_{L,max}(T) = N_{L0}\ \left(\exp\left[N_{L1}\left(\frac{1}{303} - \frac{1}{T}\right)\right]\right)\ , \tag{9}$$

where N_{L1} and N_{L0} are tunable parameters.

Note 1: The liquid volume fraction in the catalyst, $s_{ctl,an}$, represents the fraction of the membrane which is in contact with liquid water. Therefore $s_{ctl,an}$ in (6) linearly interpolates between the water content of a vapor equilibrated membrane, $\lambda_{T,a=1}$, and the liquid equilibrated value $\lambda_{max} = 22$, resolving the schroeder's paradox [13].

Note 2: There is no vapor gradient across the membrane when liquid is present in both GDLs, since the vapor concentration on both sides of the membrane is equal to $c_{v,sat}$, therefore the difference between the catalyst flooding levels $s_{ctl,an}$ and $s_{ctl,ca}$ drives water transport through the membrane.

Note 3: The membrane water diffusion coefficient, $D_w(\lambda_{mb}, T)$, has an exponential dependence on temperature, but only a linear dependence on membrane water content for values of λ_{mb} greater than 6 [17], [18]. Typical membrane water content, when the cell is near flooding conditions, is in the range 9 to 14.

The second term in (5) describes electro-osmotic drag, which pulls water from the anode to the cathode with the conduction of protons through the membrane, and therefore

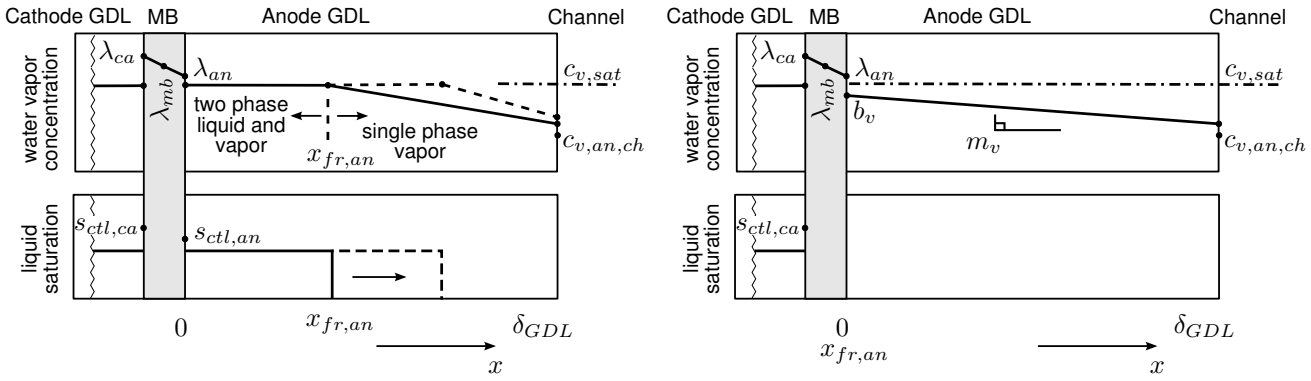

(a) Mode 2: advancing two phase front on the anode side GDL.

(b) Mode 1: only vapor phase in the GDL when $x_{fr,an} = 0$.

Fig. 3. Two phase water front evolution in the anode GDL for the unit fuel cell model, which represents a 1-D slice from Fig. 1. The figures show the assumed profiles in membrane water content (grey region), GDL water vapor concentration (upper plots) and GDL liquid water saturation (lower plots).

is dependent on the current density, i_{fc}. The drag coefficient is given by

$$n_d = \begin{cases} \lambda_{mb}/\lambda_{T,a=1} & \lambda_{mb} < \lambda_{T,a=1} \\ K_{\lambda,T}(\lambda_{mb} - \lambda_{T,a=1}) + 1 & \lambda_{mb} \geq \lambda_{T,a=1} \end{cases}, \tag{10}$$

which depends on the membrane water content and temperature with,

$$K_{\lambda,T} = \frac{(-1.834 + 0.0126\ T - 1)}{(\lambda_{max} - \lambda_{T,a=1})} \tag{11}$$

a linear interpolation between $n_d = 1$ for the vapor equilibrated membrane and $n_d = -1.834 + 0.0126\ T$, for the liquid equilibrated membrane [18].

1) Cathode Side Equations: the same set of equation are used on the cathode, with the inclusion of generated water and a change of sign which accounts for the use of a different coordinate axis,

$$\frac{1}{2}\frac{i_{fc}}{F} - N_{v,ca,mb} = N_{v,ca} + N_{l,ca}, \tag{12}$$

$$N_{v,ca,mb} = 2\,\frac{\alpha_w\, D_w(\lambda_{mb}, T)\ \cdot\ (\lambda_{ca} - \lambda_{mb})}{\delta_{mb}} - \frac{n_d\, i_{fc}}{F}. \tag{13}$$

B. GDL Water Transport

The vapor flux from the GDL to the channel, $N_{v,an}$, that defines the net flux of water accumulating inside the GDL in (3) and hence the liquid from propagation in (2) is governed by diffusion, $N_{v,an} = -D_{ve}\partial c_{v,an}/\partial x$. The GDL vapor flux takes a specific form due to the specific vapor profile assumption we made in (4),

$$N_{v,an} = -D_{ve}\ m_v. \tag{14}$$

At the GDL-Ch interface, the flux is defined by the diffusive GDL flux (at the GDL side of the GDL-ch interface)

$$N_{v,an}\big|_{\delta^-_{GDL}} = -D_{ve}\ m_v \tag{15}$$

is equal to the mass transfer type condition [15], which governs the vapor flux at the channel side of the GDL-Channel interface

$$\begin{aligned} N_{v,an}\big|_{\delta^+_{GDL}} &= k_{mt}\,(c_{v,an}(\delta_{GDL}) - c_{v,an,ch}) \\ &= k_{mt}\,(m_v\ \delta_{GDL} + b_v - c_{v,an,ch})\,, \end{aligned} \tag{16}$$

where $k_{mt} = Sh\ D_V/H_{ch}$ is the mass transfer coefficient, related to the Sherwood number Sh, the free space diffusion coefficient for vapor in hydrogen, D_V, and the characteristic length which is channel height, H_{ch}.

The equality between (15) and (16) is used to eliminate one of the vapor profile parameters, m_v. The other parameter, b_v, depends on the liquid front location $x_{fr,an}$. If ($x_{fr,an} > 0$), then the simplifying assumption $c_{v,an}(x_{fr,an}) = c_{v,sat}(T)$, and continuity of the vapor flux

$$c_{v,an}(x^-_{fr,an}) = c_{v,sat} = c_{v,an}(x^+_{fr,an}) = m_v\ x_{fr,an} + b_v\ , \tag{17}$$

allows for calculation of the vapor profile in the GDL using (15), (16) and (17) directly, as shown in (20). In order to evaluate b_v, when $x_{fr,an} = 0$ we must consider both cases arising from the $min(\cdot)$ function in (4) for the vapor concentration at the membrane. In the first case, we assume that $b_v \geq c_{v,sat}$, then $c_{v,an}(0) = \min(b_v, c_{v,sat}) = c_{v,sat}$ and we proceed as above. If $b_v < c_{v,sat}$, then $c_{v,an}(0) = b_v$ and b_v is found to satisfy a conservation of flux condition, $N_{v,an}|_{0^+} = -D_{ve}\ m_v = N_{v,an}|_{0^-} = N_{v,an,mb}$, at the MB-GDL interface, which implies $N_{L,an} = 0$ and is consistent with the assumption of sub-saturated GDL conditions. Hence, the parameter b_v forms a coupling between the vapor transport in the GDL (14) and the water transport through the membrane (5).

As an example of the evolution achieved with the equations so far, consider an increase in membrane water content λ_{mb}[1] or a change in current density that will cause an increase in b_v and a simultaneous increase in the spatial vapor gradient m_v, hence vapor flux out of the GDL. When b_v

[1]The change in λ_{mb} is here assumed to be imposed by the cathode channel conditions such as a change in the cathode inlet humidity.

reaches $c_{v,sat}(T)$, the maximum vapor flux though the GDL is achieved and any additionally flux from the membrane can not be matched by the vapor flux out of the GDL, $N_{L,an} = N_{v,an,mb} - N_{v,an} > 0$, therefore the liquid front will start advancing.

When the front location reaches to the channel $x_{fr,an} = \delta_{GDL}$, the $\min(\cdot)$ function in (2) stops the front propagation, but allows for the front to recede if the channel dries such that $c_{v,an,ch}$ decreases to a value where evaporation at the front location drives $N_{l,an} < 0$. In the case when $x_{fr,an} = \delta_{GDL}$ and $N_{l,an} > 0$, the liquid flux is transported directly into the channel, since hydrophobicity of the GDL expels water readily when $s > s_{im}$.

III. System Modes

The $\min(\cdot)$ and $\max(\cdot)$ functions in (4) and (8) lead to a switched mode system with the following physical interpretation for the resulting modes.

- Mode 1: Vapor only transport in the GDL, when there is no two phase front i.e. $x_{fr,an} = 0$ and $N_{l,an} = 0$.
- Mode 2: The two phase front is advancing, $N_{l,an} > 0$ and $x_{fr,an} \geq 0$.
- Mode 3: The two phase front is receding, $N_{l,an} \leq 0$ and $x_{fr,an} > 0$.

The dynamic equations describing membrane water content and front propagation in the GDL can be represented by one of three possible system modes for each side of the membrane.The overall system has a total of nine system modes, including the same three modes for the cathode. We consider the cathode to always be in mode 2 when a humidified air inlet is used, due to the additional product water generation at the cathode. Therefore we present the three modes relating to the anode side only.

A. Mode 1

In mode 1 there is only vapor transport in the GDL, and the dynamics of water are defined only by the membrane water content (λ_{mb}) since there is no liquid front, $x_{fr,an} = 0$. Moreover the water vapor profile changes so that the vapor flux through the GDL ($N_{v,an}$) equals the vapor flux from the membrane to the anode ($N_{v,an,mb}$), $N_{v,an,mb} = N_{v,an}$. Hence, no liquid water accumulates in the GDL, $N_{L,an} = 0$, and consequently $\dot{x}_{fr,an} = 0$. The water vapor profile and its associated flux though the GDL can be calculated in this mode using (5) where ($c_{v,an}(0) = b_v$) is used in the calculation of, λ_{an}, as described in II-A, which reduces to

$$\lambda_{an} = \lambda\left(T, a\right), \text{ and } a = \frac{b_v}{c_{v,sat}}. \tag{18}$$

An additional simplification is achieved by linearization of the water uptake,

$$\lambda\left(T, a\right) \approx m_\lambda(T)\, a + b_\lambda(T) \tag{19}$$

which allows us to derive a closed form solution for $N_{v,an,mb}$ from (4, 5, 15, 16) and (19). The resulting flux is shown in (25).

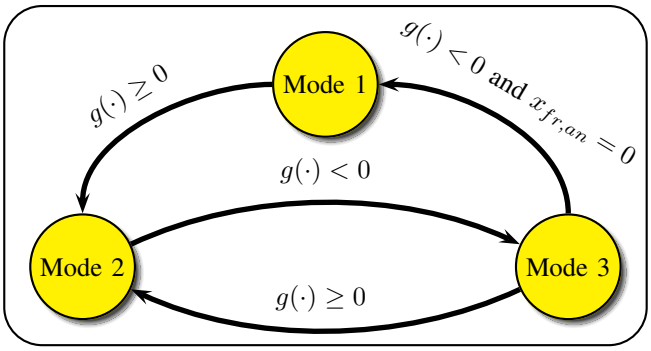

Fig. 4. Hybrid state model of advancing ($g > 0$) and receding ($g \leq 0$) water fronts in the GDL.

Note 4: The temperature dependent parameters m_λ, and b_λ, are found by linearizing the membrane uptake isotherm, (7), around the point $a = 1$. For very dry regions of the fuel cell, away from $a = 1$, this linearization may be inaccurate and hence should be replaced by the actual cubic uptake isotherm. In this case, calculation of $N_{v,an,mb}$ using iterative numerical solution strategy could be employed.

B. Modes 2 & 3

The presence of liquid water in the GDL for modes 2 & 3 decouple vapor transport in the GDL from membrane water transport. Evaluation of the vapor profile (4) at the front location (17) allows direct calculation of the vapor flux. Solution of (17), (15), and (16), yields the vapor flux through the GDL which is valid for both modes 2 and 3,

$$N^{(2)}_{v,an} = N^{(3)}_{v,an} = \frac{D_{ve}\, k_{mt}\, \left(c_{v,sat} - c_{v,an,ch}\right)}{D_{ve} + k_{mt}\left(\delta_{GDL} - x_{fr,an}\right)}\,. \tag{20}$$

Calculation of the vapor flux from the membrane to the GDL, $N_{v,an,mb}$, depends on the water activity at the MB-GDL interface. Since liquid water is present in the GDL, $a = 1$ in (6) independently of $N_{v,an}$. The $\max(\cdot)$ function in (8) leads to different dynamic system behavior for modes 2 and 3. In mode 3 (receding front), $N_{l,an} \leq 0$ and $s_{ctl,an} = 0$ by (8), therefore simultaneous solution of (5-6), yields a simple relationship for the membrane water flux though the anode side of the membrane,

$$N^{(3)}_{v,an,mb} = \frac{2\,\alpha_w\, D_w(\lambda_{mb}, T)\,(\lambda_{mb} - \lambda_{T,a=1})}{\delta_{mb}} - \frac{n_d\, i_{fc}}{F}\,. \tag{21}$$

The solution of (5-9) for mode 2 is shown in (26).

IV. Hybrid Modes and Switching Conditions.

The dynamic evolution of the two phase liquid-vapor front in the anode GDL ($x_{fr,an}$) can be described by a hybrid dynamical system with three distinct modes, as shown in Fig. 4. The transitions between these modes are determined by the states (the front location $x_{fr,an}$ and the membrane water content λ_{mb}) and the inputs (channel water vapor concentration $c_{v,an,ch}$ and current density i_{fc}) through the switching function $g(\cdot)$,

$$g(x_{fr,an}, c_{v,an,ch}, \lambda_{mb}, i_{fc}) = N^{(3)}_{v,an,mb} - N^{(2)}_{v,an}. \tag{22}$$

- Mode 1: $x_{fr,an} = 0$ and $N_{l,an} = 0$, Vapor transport only. (3) reduces to $N_{v,an} = N_{v,an,mb}$

$$N^{(1)}_{v,an,mb} = -\frac{D_{ve}\, k_{mt} \left(2\, \alpha_w\, D_w(\lambda_{mb}, T)\, F\, \left(-c_{v,sat}\, \lambda_{mb} + c_{v,an,ch}\, m_\lambda + c_{v,sat}\, b_\lambda\right) + n_d\, c_{v,sat}\, \delta_{mb}\, i_{fc}\right)}{F\, \left(k_{mt}\, c_{v,sat}\, D_{ve}\, \delta_{mb} + 2\, D_{ve}\, m_\lambda\, \alpha_w\, D_w(\lambda_{mb}, T) + 2\, k_{mt}\, \delta_{GDL}\, m_\lambda\, \alpha_w\, D_w(\lambda_{mb}, T)\right)} \tag{25}$$

- Mode 2: $x_{fr,an} \geq 0$ and $N_{l,an} > 0$, two phase transport with $s_{ctl,an} > 0$. The vapor flux is given by (20).

$$\begin{aligned} N^{(2)}_{v,an,mb} = &\left[N_{l,max}\, \left(n_d\, i_{fc}\, \delta_{mb} - 2\, \alpha_w\, D_w(\lambda_{mb}, T)\, F\, \left(\lambda_{mb} - \lambda_{T,a=1}\right)\right)\, \left(D_{ve} + k_{mt}\, \left(\delta_{GDL} - x_{fr,an}\right)\right)\right. \\ &\left. + 2\, \alpha_w\, D_w(\lambda_{mb}, T)\, D_{ve}\, k_{mt}\, F\, \left(\lambda_{T,a=1} - \lambda_{max}\right)\, \left(c_{v,sat} - c_{v,an,ch}\right)\right] \\ &* \left[F\, \left(D_{ve} + k_{mt}\, \left(\delta_{GDL} - x_{fr,an}\right)\right)\, \left(2\, \alpha_w\, D_w(\lambda_{mb}, T)\, \left(\lambda_{T,a=1} - \lambda_{max}\right) - N_{l,max}\, \delta_{mb}\right)\right]^{-1} \end{aligned} \tag{26}$$

The switching function $g(\cdot)$ compares the vapor flux, assuming an advancing front, mode 2, using (20) to the membrane flux at the transition between modes 1, 2 and 3, which is equivalent to the membrane flux in mode 3 using (21), by assuming a stationary front $N_{L,an} = 0$ as shown below.

When $(x_{fr,an} > 0)$

$$\lim_{N_{L,an} \to 0^+} N_{v,an,mb} = \lim_{\lambda_{an} \to \lambda_{T,a=1}} N^{(2)}_{v,an,mb} = N^{(3)}_{v,an,mb} \tag{23}$$

and when $(x_{fr,an} = 0)$

$$\lim_{N_{L,an} \to 0^-} N_{v,an,mb} = \lim_{b_v \to c_{v,sat}} N^{(1)}_{v,an,mb} = N^{(3)}_{v,an,mb} \tag{24}$$

If $g(\cdot) > 0$ then the front must be advancing, and the system is in mode 2, otherwise the front is receding and the system is in mode 3 until the front reaches the membrane $(x_{fr,an} = 0)$, at which point the system switches to mode 1.

V. Conclusions and Future Work

In this paper, a hybrid dynamical model for the advancing and receding two phase liquid-vapor fronts in the GDL of a PEMFC was presented. Three system modes, are required to describe the advancing front, receding front and vapor only phase in the anode GDL. Several simplifying assumptions were presented in order to describe the slowly evolving liquid water dynamics using ODEs, which yields a huge reduction in the computational complexity of the model when compared to the traditional approach of solving the coupled two-phase diffusion partial differential equation. The inclusion of catalyst flooding and the resulting impact on membrane water transport highlights another improvement over our previous work. The model can be used to estimate the membrane water content, the rate of water crossover though the membrane and liquid water accumulation in the anode channel, all of which impact fuel cell performance.

Our next goal is the development of an along the channel moving front similar to [16] and parameterization of the tunable parameters, (such as D_{ve} in (14), $N_{L,0}$ and $N_{L,1}$ in (9), α_w in (5) and s_* in (2)), to match measurements of liquid water accumulation in PEMFC via neutron imaging [1].

References

[1] J. B. Siegel, D. A. McKay, A. G. Stefanopoulou, D. S. Hussey, and D. L. Jacobson, "Measurement of liquid water accumulation in a PEMFC with dead-ended anode," *Journal of The Electrochemical Society*, vol. 155, pp. B1168–B1178, 2008.

[2] S. S. Kocha, J. D. Yang, and J. S. Yi, "Characterization of gas crossover and its implications in PEM fuel cells," *AIChE Journal*, vol. 52, no. 5, pp. 1916–1925, 2006.

[3] E. Mueller, F. A. Kolb, A. G. Stefanopoulou, D. A. McKay, and L. Guzzella, "Correlating Nitrogen Accumulation with Temporal Fuel Cell Performance," in *Proc. of Dynamic Systems and Control Conference (DSCC08)*, ser. , Paper TuAT5.1, 2008.

[4] E. Kimball, T. Whitaker, Y. G. Kevrekidis, and J. B. Benziger, "Drops, slugs, and flooding in polymer electrolyte membrane fuel cells," *AIChE Journal*, vol. 54, no. 5, pp. 1313–1332, 2008.

[5] W. Baumgartner, P. Parz, S. Fraser, E. Wallnfer, and V. Hacker, "Polarization study of a PEMFC with four reference electrodes at hydrogen starvation conditions," *Journal of Power Sources*, vol. 182, no. 2, pp. 413–421, Aug. 2008.

[6] S. Hikita, F. Nakatani, K. Yamane, and Y. Takagi, "Power-generation characteristics of hydrogen fuel cell with dead-end system," *JSAE Review*, vol. 23, pp. 177–182, 2002.

[7] P. Rodatz, A. Tsukada, M. Mladek, and L. Guzzella, "Efficiency Improvements by Pulsed Hydrogen Supply in PEM Fuel Cell Systems," in *Proceedings of IFAC 15th World Congress*, 2002.

[8] D. A. McKay, J. B. Siegel, W. Ott, and A. G. Stefanopoulou, "Parameterization and prediction of temporal fuel cell voltage behavior during flooding and drying conditions," *Journal of Power Sources*, vol. 178, no. 1, pp. 207–222, Mar. 2008.

[9] J. Siegel, D. McKay, and A. Stefanopoulou, "Modeling and validation of fuel cell water dynamics using neutron imaging," in *American Control Conference, 2008*, 2008, pp. 2573–2578.

[10] B. A. McCain, A. G. Stefanopoulou, and I. V. Kolmanovsky, "On the dynamics and control of through-plane water distributions in pem fuel cells," *Chemical Engineering Science*, vol. 63, no. 17, pp. 4418–4432, Sep. 2008.

[11] A. Z. Weber and J. Newman, "Transport in Polymer-Electrolyte Membranes I. Physical Model," *J. Electrochem. Soc.*, vol. 150, no. 7, pp. A1008–A1015, Jul. 2003.

[12] A. Shah, G.-S. Kim, P. Sui, and D. Harvey, "Transient non-isothermal model of a polymer electrolyte fuel cell," *Journal of Power Sources*, vol. 163, no. 2, pp. 793 – 806, 2007.

[13] L. M. Onishi, J. M. Prausnitz, and J. Newman, "Water-nafion equilibria. absence of schroeder's paradox," *The Journal of Physical Chemistry B*, vol. 111, no. 34, pp. 10 166–10 173, 2007.

[14] J. Nam and M. Kaviany, "Effective diffusivity and water-saturation distribution in single and two-layer PEMFC diffusion medium," *Int. J. Heat Mass Transfer*, vol. 46, pp. 4595–4611, 2003.

[15] Z. H. Wang, C. Y. Wang, and K. S. Chen, "Two-phase flow and transport in the air cathode of proton exchange membrane fuel cells," *J. Power Sources*, vol. 94, no. 1, pp. 40–50, Feb. 2001.

[16] K. Promislow, P. Chang, H. Haas, and B. Wetton, "Two-phase unit cell model for slow transients in polymer electrolyte membrane fuel cells," *Journal of The Electrochemical Society*, vol. 155, no. 7, pp. A494–A504, 2008.

[17] S. Ge, X. Li, B. Yi, and I.-M. Hsing, "Absorption, desorption, and transport of water in polymer electrolyte membranes for fuel cells," *Journal of The Electrochemical Society*, vol. 152, no. 6, pp. A1149–A1157, 2005.

[18] S. Ge, B. Yi, and P. Ming, "Experimental determination of electro-osmotic drag coefficient in nafion membrane for fuel cells," *Journal of The Electrochemical Society*, vol. 153, no. 8, pp. A1443–A1450, 2006.